remote sensing

MDPI

Technical Note

Inter-Satellite Single-Difference Ionospheric Delay Interpolation Model for PPP-RTK and Its Positioning Performance Verification

Ju Hong [1,2], Rui Tu [1,2,3,*], Shixuan Zhang [1,2], Fangxin Li [1,2], Mingyue Liu [1,2] and Xiaochun Lu [1,2,3]

[1] National Time Service Center, Chinese Academy of Sciences, Shu Yuan Road, Xi'an 710600, China
[2] University of Chinese Academy of Sciences, Yu Quan Road, Beijing 100049, China
[3] Key Laboratory of Precision Navigation and Timing Technology, Chinese Academy of Sciences, Shu Yuan Road, Xi'an 710600, China
* Correspondence: turui@ntsc.ac.cn

Abstract: In PPP-RTK, obtaining accurate atmospheric delay information for the user through interpolation is one of the keys to achieving high-precision real-time positioning. The ionospheric delay that is extracted by a reference network based on uncalibrated phase delay (UPD) products is often difficult to separate from errors such as receiver code hardware delay and UPD reference error. Inter-satellite single-difference (SD) ionospheric delay information is typically provided to the user. This paper proposes an interpolation model that uses the atmospheric delay coefficient to represent the SD ionospheric delay, based on the mean position of the ionospheric pierce point (IPP) of each satellite pair and the center position of the network, which is called the differenced surface model (DSM). We chose four scenarios to compare the interpolation accuracy of the proposed model with the inverse distance-based linear interpolation method (DIM) and USM based on the difference between the longitude and latitude of the reference and ionospheric pierce point (IPP) of every satellite (here, we call it USM for short). The four scenarios involve a medium-scale reference network with an average distance to the reference station of 41 km, a large-scale reference network with an average distance to the reference station of 98 km, and out-of-network users, and a network with a common minimum of three reference stations. The results show that the root mean square (RMS) of the SD residuals of ionospheric delay for DSM were 1.4, 3.2, 2.2, and 1.4 cm, respectively, for the four scenarios that were considered, which are slightly better delay values than those that were achieved using DIM and USM. For the scenario with three reference stations, the interpolation accuracies of DIM and DSM were no different from those for four reference stations, indicating that the server can still try to provide ionospheric correction service under the condition of fewer reference stations. In contrast, USM could not provide service because it lacked the sufficient number of reference stations. DSM was used as the ionospheric delay interpolation model to analyze GPS and Galileo dual-system PPP-RTK positioning performance. In addition, the atmospheric parameter constraint method of users was used in PPP-RTK in reference networks of different scales. For the 41-km and 98-km reference networks, the time to first fix (TTFF) were 14.5 s and 33.1 s, respectively, and the mean RMS values for the east (E), north (N), and up (U) directions were 0.80, 0.93, and 2.72 cm, respectively, and 1.0, 1.1, and 4.0 cm, respectively, for a period of 5 min after convergence. The fixing rate and positioning accuracy of DSM during the 5-min period were better than those of DIM when the same empirical model was used to determine the mean square error of atmospheric delay.

Keywords: PPP-RTK; inter-satellite single-difference ionospheric delay; regional interpolation model; positioning performance

check for updates

Citation: Hong, J.; Tu, R.; Zhang, S.; Li, F.; Liu, M.; Lu, X. Inter-Satellite Single-Difference Ionospheric Delay Interpolation Model for PPP-RTK and Its Positioning Performance Verification. *Remote Sens.* **2022**, *14*, 4153. https://doi.org/10.3390/rs14174153

Academic Editor: Stefania Bonafoni

Received: 20 June 2022
Accepted: 19 August 2022
Published: 24 August 2022

Publisher's Note: MDPI stays neutral with regard to jurisdictional claims in published maps and institutional affiliations.

Copyright: © 2022 by the authors. Licensee MDPI, Basel, Switzerland. This article is an open access article distributed under the terms and conditions of the Creative Commons Attribution (CC BY) license (https://creativecommons.org/licenses/by/4.0/).

1. Introduction

Compared with PPP (precise point positioning) technology, PPP that is based on real-time kinematic (RTK) network (PPP-RTK) technology can enable rapid integer ambiguity

resolution (IAR) by exploiting precise atmospheric delay information that is provided by a regional network [1–3] and has unique advantages in convergence, accuracy, and real-time communication. As a result, PPP-RTK technology has received considerable attention. Compared with representation in an observation space in an RTK network, PPP-RTK provides state-space data that can be modeled and broadcast to users according to the different physical characteristics of the corrections. Obtaining accurate atmospheric delay information for users by means of an interpolation model in PPP-RTK is one of the keys to achieving high-precision real-time positioning. The atmospheric delay errors which are related to distance increase with increasing distance between user stations and reference stations. Therefore, the commonly used interpolation models all consider the correlation and uniformity of space. The most commonly used distance interpolation models are the distance-based linear interpolation model (LIM) [4], inverse distance-based linear interpolation method (DIM) [5], linear combination model (LCM) [6,7], low-order surface model (LSM) [8,9], least-squares collocation (LSC) method [10,11], and kriging interpolation method [12,13]. Dai et al. [14] compared these methods and concluded that their performance was not significantly different. Wang et al. [15] analyzed the interpolation accuracy of different interpolation models and gave the best reference results under different scales and terrain scenarios. Li et al. [16] proposed the modified LCM (MLCM), which is based on the LCM but with a different method for selecting the reference for interpolation coordinates. The MLCM method changes the reference coordinate from any reference station of the LCM method to the user station. Otherwise, the two methods are theoretically equivalent. Zhu et al. [17] considered the latitude and longitude anisotropy of the ionospheric total electron content (TEC) distribution by introducing latitude and longitude adjustment factors to improve the accuracy of inverse distance weighting interpolation. Cui et al. proposed a version of LIM that was based on coinciding ionospheric pierce points (CIPPs) to improve the interpolation accuracy of ionospheric delays in low-latitude regions [18]. The inter-satellite single difference (SD) ionospheric delay is typically provided to the user. Unless specified otherwise, SD is the single difference between satellites. Wu et al. [19] constructed an atmospheric delay model using the longitude and latitude of the network center and IPP, and broadcast the atmospheric delay correction coefficient for users (referred to as the USM). This method requires at least four stations and four satellites to solve the model coefficients. In regional enhanced PPP, the common function-based ionospheric interpolation methods such as LCM, DIM, LSM, LIM, and USM have advantages and disadvantages, and have application examples.

There are few studies on the model of ionospheric delay that is expressed by the atmospheric delay coefficient based on the IPP in the region enhancement algorithm, which is worthy of further exploration. This paper proposes an interpolation model that uses the atmospheric delay coefficient to represent the SD ionospheric delay, based on the mean position of the ionospheric pierce point (IPP) of the satellite pair and the center position of the network, which is called the differenced surface model (DSM). When the number of stations is at least three, the ionospheric delay model coefficients of any single-difference satellite pair can be calculated. In this study, the interpolation performance of DIM, USM, and the new DSM model was compared for different scenarios. In addition, DIM was selected for comparison with DSM in an analysis of PPP-RTK positioning performance for typical medium- and large-scale reference networks.

We first introduce the algorithms of the interpolation models and the extraction of server-side atmospheric delay and constraint of user-side atmospheric delay. The data processing strategies are then presented. Finally, we present an analysis of the accuracy of the proposed interpolation model versus other models and the performance of PPP-RTK at the user end for different scenarios.

2. Methodology

2.1. Interpolation Model

The interpolation accuracy of the proposed DSM was compared with that of the commonly used DIM as well as USM which is based on the longitude and latitude of the network center and IPP. The LSM can consider various forms, such as elevation, to adapt to different application environments, so it was chosen as an interpolation function of tropospheric delay that is sensitive to elevation. The interpolation model that was used is described below.

2.1.1. DIM

DIM can be expressed as a linear combination of a set of reference station corrections, and the combination coefficient is the reciprocal of the distance. When there are n reference stations, the mathematical model is as follows [5]:

$$A_u = \sum_{i=1}^{n} \alpha_i \cdot A_i \tag{1}$$

where A_u represent the atmospheric delay interpolations of the user, i represents the reference station, u represents the user station, $\alpha = \begin{bmatrix} p_1/p & p_2/p & \cdots & p_n/p \end{bmatrix}$ represents the interpolation coefficients, and p_i is the reciprocal of the distance between a reference station and a user station and $p = \sum_{i=1}^{n} p_i$. DIM is related to the geometric distribution of user stations and reference stations, as well as the geometric relationship between reference stations and satellites, and has nothing to do with interpolation.

2.1.2. LSM

LSM is based on the coefficient representing the trend of the corrections, and the coefficients are calculated by least-squares that is performed on data that are generated by the reference network. Taking the first-order form as an example, the mathematical model is as follows [15]:

$$A_i = \alpha_1 \Delta X_{i,u} + \alpha_2 \Delta Y_{i,u} + \alpha_3 \tag{2}$$

where A_i represents the atmospheric delay, i represents the station; $\Delta X_{i,u} = X_i - X_u$, $\Delta Y_{i,u} = Y_i - Y_u$ and X, Y are the plane coordinates of the station; and α_1, α_2 and α_3 represent model coefficients. LSM can choose whether to add an elevation factor, and the fitting order can be selected in first-order or second-order forms to adapt to different application environments. The interpolation coefficient is related to the position and atmospheric delay of the reference stations.

2.1.3. USM

The coefficients and value of atmospheric delay are two ways to express the trend of atmospheric delay. According to the characteristics of atmospheric delay, the USM constructs the atmospheric delay by using the longitude and latitude of the network center and IPP. Each satellite model can be expressed as follows [19]:

$$\overline{A}_i^p = a_0^p + a_1^p \cdot (\varphi_p - \varphi_0) + a_2^p \cdot (\lambda_p - \lambda_0) \tag{3}$$

where $\overline{A}_i^p$ represents the atmospheric delay of the station i and the satellite p. The SD ionospheric delay interpolation can be expressed as follows:

$$\Delta \overline{I}_i^{p,q} = (a_0^p + a_1^p \cdot (\varphi_p - \varphi_0) + a_2^p \cdot (\lambda_p - \lambda_0)) - (a_0^q + a_1^q \cdot (\varphi_q - \varphi_0) + a_2^q \cdot (\lambda_q - \lambda_0)) \tag{4}$$

In this equation, q represents the reference satellite; p represents other satellites; φ_p and λ_p represent the latitude and longitude of the IPP of satellite p, respectively; φ_q and λ_q represent the latitude and longitude of the IPP of satellite q, respectively; φ_0 and λ_0 represent the latitude and longitude of the center of the network, respectively; a_0, a_1, and a_2

are model coefficients; and $\Delta\bar{I}_i^{p,q}$ represents the SD ionospheric delay. This method requires at least four stations and four satellites to solve for the model coefficients.

2.1.4. DSM

Unlike USM, which requires the overall least squares of all satellites in the same system to solve for the atmospheric delay coefficients of each satellite, this paper proposes an SD ionospheric surface model based on the mean value of the IPP of the satellite pair and the center position of the reference station. When the number of reference stations is at least three, the atmospheric delay model coefficient (DSM) of any single-difference satellite pair can be calculated. The mathematical model is as follows:

$$\Delta\bar{I}_i^{p,q} = a_0^{p,q} + a_1^{p,q}\cdot(\frac{\varphi_q+\varphi_p}{2} - \varphi_0) + a_2^{p,q}\cdot(\frac{\lambda_q+\lambda_p}{2} - \lambda_0) \tag{5}$$

where $a_0^{p,q}$, $a_1^{p,q}$, and $a_2^{p,q}$ represent model coefficients of the satellite p and q. The definitions of other terms in this equation are the same as for the previous Equation (4). After the user receives the atmospheric delay coefficient, the same formula can be used to calculate the atmospheric delay of any single difference. When solving for the USM and DSM coefficients, each system selects a reference satellite. The user side uses the same method to restore the ionospheric delay of any satellite pair when applying coefficients.

2.2. Extraction and Constraints of Atmospheric Delay

2.2.1. Server-Side Atmospheric Delay Extraction

The server selects the ionosphere-free model to fix the SD ambiguity and extracts the atmospheric delay correction. The equations for raw code and phase observations are as follows [20]:

$$\begin{cases} P_{r,i}^s = \rho_r^s + ct_r - ct^s + \gamma_i I_{r,1}^s + T_r^s + d_{r,i} - d_i^s + \varepsilon_{P,r,i}^s \\ L_{r,i}^s = \rho_r^s + ct_r - ct^s - \gamma_i I_{r,1}^s + T_r^s + \lambda_i N_{r,i}^s + b_{r,i} - b_i^s + \varepsilon_{L,r,i}^s \end{cases} \tag{6}$$

where the subscript i, r, and s represent the frequency, reference station, and satellite, respectively; P and L are the code and phase measurements, respectively; t_r and t^s are the receiver clock error and satellite clock error, respectively; I and T represent the ionospheric and tropospheric delay, respectively; $d_{r,i}$ and d_i^s represent the receiver and satellite code hardware delays, respectively; $b_{r,i}$ and b_i^s represent the receiver and satellite phase hardware delays, respectively; ε represents observation noise, multipath effects, and other unmodeled errors; λ is the wavelength of the carrier phase; N is the integer ambiguity; c is the speed of light; and $\gamma_i = (\lambda_i/\lambda_1)^2$. The tropospheric model delay T_r^s can be written as follows:

$$T_r^s = M_{h,r}^s d_{h,r} + M_{w,r}^s d_{w,r} \tag{7}$$

where $d_{h,r}$ and $d_{w,r}$ are the dry and wet delays of the site-specific zenith tropospheric delay, respectively, and $M_{h,r}^s$ and $M_{w,r}^s$ are the mapping functions of dry and wet delay, respectively. After error correction and reparameterization, the ionospheric-free (IF) dual-frequency combined observation equation is as follows:

$$\begin{cases} p_{r,IF}^s = \mu_r^s\cdot x + c\bar{t}_r - c\bar{t}^s + M_{w,r}^s d_{w,r} + \varepsilon_{P,r,IF}^s \\ l_{r,IF}^s = \mu_r^s\cdot x + c\bar{t}_r - c\bar{t}^s + M_{w,r}^s d_{w,r} + \lambda_1\overline{N}_{r,IF}^s + \varepsilon_{\Phi,r,IF}^s \end{cases} \tag{8}$$

In the formula,

$$\begin{cases} c\bar{t}_r = ct_r + d_{r,IF} \\ c\bar{t}^s = ct^s + d_{IF}^s \\ \lambda_1\overline{N}_{r,IF}^s = \lambda_1 N_{r,IF}^s + b_{r,IF} - b_{IF}^s - d_{r,IF} + d_{IF}^s \end{cases}$$

where μ_r^s is the unit vector of the component from the receiver to the satellite and x is the vector of the receiver position increments relative to the a priori position. The precise satellite clock error product was used to correct satellite clock error, which includes satellite clock error and ionosphere-free code hardware delay of satellites. The server extracts the tropospheric delay and ionospheric delay using coordinate constraints and ambiguity fixing methods and uses the IF observations to invert the tropospheric wet delay component.

$$\overline{T}_{w,r}^s = L_{r,IF}^s - \rho_r^s - c\bar{t}_r + c\bar{t}^s - \lambda_1 \overline{N}_{r,IF}^s - M_{h,r}^s d_{h,r} \tag{9}$$

If the noise term is ignored, the ionospheric delay correction can be calculated as follows:

$$\overline{I}_1^s = \rho_r^s + c\bar{t}_r - c\bar{t}^s + \left(M_{h,r}^s d_{h,r} + \overline{T}_{w,r}^s\right) + \lambda_1 N_1^s + b_{r,1} - b_1^s - L_{r,1}^s \tag{10}$$

The UPD product can correct the hardware delay in the equation. The ionospheric delay can be expressed as follows:

$$\overline{I}_1^s = I_{r,1}^s + \delta Z \tag{11}$$

where $I_{r,1}^s$ is the theoretical ionospheric delay, and δZ represents common satellite errors, including errors such as the UPD product benchmark and receiver code hardware delay.

2.2.2. User-End Atmospheric Delay Constraints

In medium-scale and long-scale reference station networks, the spatial correlation of atmospheric delay is greatly reduced. If the user uses the atmospheric delay of reference stations directly, the residuals are absorbed by the ambiguity and affect fast IAR. To eliminate the influence of receiver-related errors in the ionospheric delay, the SD ionospheric and zenith tropospheric delay corrections are introduced into the undifferenced and uncombined (UDUC) PPP as virtual observations. If the receiver code hardware delay cannot be reasonably handled, the performance in a PPP application may be degraded [21–23]. By adding the ionospheric a priori correction information constraint, the receiver code hardware delay can be estimated. Assuming that m satellites are observed and that the fth satellite is selected as the reference satellite, the dual-frequency UDUC PPP functions with external atmospheric corrections after error correction and reparameterization can be expressed as follows:

$$\begin{cases} p_{u,1}^{s1} = \mu_u^{s1} \cdot x + c\bar{t}_u - c\bar{t}^{s1} + M_{w,u}^{s1} d_{w,u} + I_{u,1}^{s1} + \varepsilon_{P,u,1}^{s1} + \gamma_2^2 / \left(\gamma_2^2 - 1\right) DCB_u \\ p_{u,2}^{s1} = \mu_u^{s1} \cdot x + c\bar{t}_u - c\bar{t}^{s1} + M_{w,u}^{s1} d_{w,u} + \gamma_2 I_{u,1}^{s1} + \varepsilon_{P,u,2}^{s1} - 1 / \left(1 - \gamma_2^2\right) DCB_u \\ l_{u,1}^{s1} = \mu_u^{s1} \cdot x + c\bar{t}_u - c\bar{t}^{s1} + M_{w,u}^{s1} d_{w,u} - I_{u,1}^s + \lambda_1 \overline{N}_{u,1}^s + \varepsilon_{\Phi,u,1}^{s1} \\ l_{u,2}^{s1} = \mu_u^{s1} \cdot x + c\bar{t}_u - c\bar{t}^{s1} + M_{w,u}^{s1} d_{w,u} - \gamma_2 I_{u,2}^{s1} + \lambda_2 \overline{N}_{u,2}^{s1} + \varepsilon_{\Phi,u,2}^{s1} \\ \quad \vdots \\ p_{u,1}^{sm} = \mu_u^{sm} \cdot x + c\bar{t}_u - c\bar{t}^{sm} + M_{w,u}^{sm} d_{w,u} + I_{u,1}^{sm} + \varepsilon_{P,u,1}^{sm} + \gamma_2^2 / \left(\gamma_2^2 - 1\right) DCB_u \\ p_{u,2}^{sm} = \mu_u^{sm} \cdot x + c\bar{t}_u - c\bar{t}^{sm} + M_{w,u}^{sm} d_{w,u} + \gamma_2 I_{u,1}^{sm} + \varepsilon_{P,u,2}^{sm} - 1 / \left(1 - \gamma_2^2\right) DCB_u \\ l_{u,1}^{sm} = \mu_u^{sm} \cdot x + c\bar{t}_u - c\bar{t}^{sm} + M_{w,u}^{sm} d_{w,u} - I_{u,1}^{sm} + \lambda_1 \overline{N}_{u,1}^{sm} + \varepsilon_{\Phi,u,1}^{sm} \\ l_{u,2}^{sm} = \mu_u^{sm} \cdot x + c\bar{t}_u - c\bar{t}^{sm} + M_{w,u}^{sm} d_{w,u} - \gamma_2 I_{u,1}^{sm} + \lambda_2 \overline{N}_{u,2}^{sm} + \varepsilon_{\Phi,u,2}^{sm} \\ \Delta \overline{I}_{u,1}^{s1,sf} = I_{u,1}^{s1} - I_{u,1}^{sf} \\ \quad \vdots \\ \Delta \overline{I}_{u,1}^{sm-1,sf} = I_{u,1}^{sm-1} - I_{u,1}^{sf} \\ \overline{d}_{wet,u} = d_{w,u} \end{cases} \tag{12}$$

In the formula,

$$\lambda_i \overline{N}^s_{u,i} = \lambda_1 N^s_{r,i} + b_{r,i} - b^s_i + d^s_{IF}$$

where u represents the user station, $\Delta\overline{I}$ is the SD ionospheric delay, $\overline{d}_{w,u}$ is the tropospheric zenith wet delay, and the other terms in the equation are as defined previously. The users and servers use the same data processing method to ensure consistency.

3. Experimental Data and Processing Strategies

The interpolation accuracy of the new model was examined for four different application scenarios: a medium-scale reference network with an average distance of 41 km, a large-scale reference network with an average distance of 98 km, out-of-network users, and a network with a typical minimum of three reference stations. In addition, two typical scenarios of medium-scale and large-scale reference networks were selected to test and analyze the PPP-RTK positioning performance. Details of the data processing strategies are shown in Table 1. Both USM and DSM select the satellite with the highest elevation angle as the reference satellite to calculate the interpolation coefficient. The code and carrier observations were still modeled randomly based on the elevation angle at the service and user end. The empirical value was used to determine the weight of tropospheric zenith delay and ionospheric delay in the test [24,25].

Table 1. Models and strategies that were adopted.

Items	Model and Strategies
Frequency selection	GPS: L1/L2 GALILEO: E1/E5a
Observations	Server: IF observations of carrier phase and code observation User: uncombined phase and code observation
Sampling rate	5 s
Estimator	Kalman filtering
Cut-off elevation angle	Float: 7° Fix: 10°
Station coordinates	Server: Estimated as constants in static mode User: Estimated as constants in dynamic mode
Ionospheric delay	Server: Eliminated by IF observations User: Constraint + Estimated
Phase ambiguities	Server: WL + NL partial fixing User: WL + L1/L2 partial fixing
Tropospheric delay	Dry component: Corrected by Saastamoinen model with NMF mapping function Wet component: (1) Server: Estimated by as piece-wise constant with NMF mapping function (2) User: Constraint + Estimated by as piece-wise constant with NMF mapping function
Satellite orbit and clock	Using the precise products from GFZ
Satellite and receiver antenna phase center	igs14.atx
Tidal loading, Ocean tide, Earth rotation effects, Phase wind-up effect	Model correction

CORS data for the United States were selected for testing and analysis. The distribution of the stations is shown in Figure 1. For the medium-scale network that is illustrated in Figure 1a, the distances between the user station and the reference stations are 30–55 km, with a maximum distance of 52.6 km and an average distance of 41 km. This was considered scenario A. For the large-scale network that is illustrated in Figure 1b, the distances between

the user station and the reference stations in the reference network are in the range of 90–105 km, with a maximum distance of 103.2 km and an average distance of 98 km. This was considered scenario B. The ncta/ncec/ncgo/ncwl stations in Figure 1 were selected as reference stations, and the ncsf station was selected as the user station to analyze the interpolation accuracy when the user was outside the network. The average distance from the user station to a reference station was 58.5 km. This was considered scenario C. With the ncta/ncec/ncsf stations in Figure 1a selected as reference stations, the ncwl station was selected as the user station to analyze the interpolation accuracy when there were three reference stations. The average distance from the user station to a reference station was 43.5 km. This was considered scenario D. The data collection time interval was UTC 1:00–23:30 on 21 December 2021, with an epoch interval of 5 s.

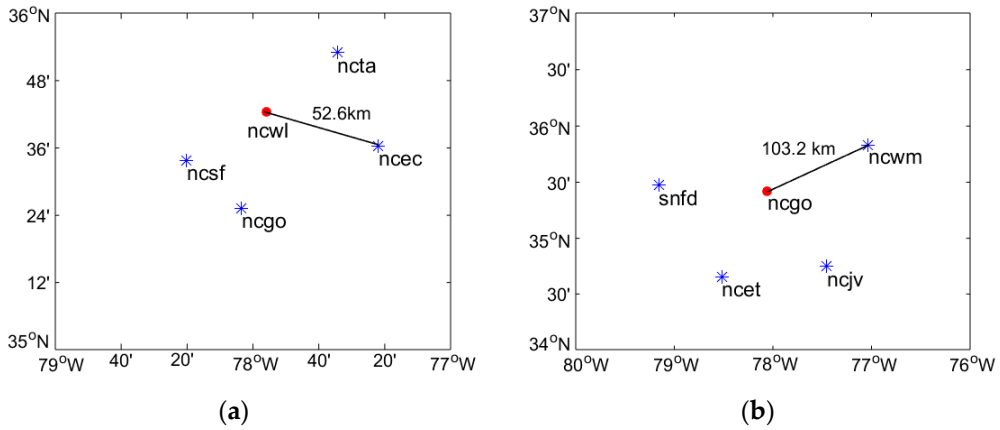

Figure 1. Distribution of stations. (**a**) The distribution of medium-scale reference networks; (**b**) the distribution of large-scale reference networks. The blue asterisks represent reference stations and red dots represent user stations.

4. Results

4.1. Accuracy Analysis of Interpolation Model

Using the same data processing strategy as that for the user, the atmospheric delay was extracted through the fixed ambiguity, and the difference between the extracted value and the interpolation was used to evaluate the internal coincidence accuracy. Figure 2 shows the residuals of ionospheric delay for scenario A. The common discontinuity of the three model epochs was caused by the lack of fixed-ambiguity common-view satellites at the reference stations. Compared with the other two models, USM had other discontinuous epochs. This was because there were less than four common-view GPS satellites with fixed ambiguity, and the interpolation coefficient could not be calculated. Most of the ionospheric delay residuals of the three models are within 0.1 m, and the residuals of the USM model exceed 0.1 m in some epochs. The ionospheric delay residual became significantly larger during 9:00–16:00 local time. The results for the three models were relatively similar for other scenarios and were not displayed.

Table 2 shows the root mean square (RMS) and standard deviation (STD) values of the SD ionospheric residuals of all satellites for the three models. It can be seen that the ionospheric residuals of the three models increase with increasing distance between the user station and the reference station in scenarios A and B. The RMS values of the SD ionospheric delay residuals for DSM for the 41-km and 98-km reference networks were 1.4 cm and 3.2 cm, respectively. In the scenario in which the user station outside the network was 33 km away from the nearest reference station, the RMS and STD values of ionospheric residuals for DSM were 2.2 cm. The interpolation accuracy of DSM was slightly better than DIM and USM in both scenarios. As can be seen in Figure 3, the USM performed the worst in the B, and the interpolation accuracy of DSM is 34.7% higher than that of the USM. In other scenarios, the interpolation accuracy of USM is similar to that of DIM, the

interpolation accuracy of DSM is 22.2%, 25.6%, 24.1%, and 22.2% higher than DIM in the four types, respectively.

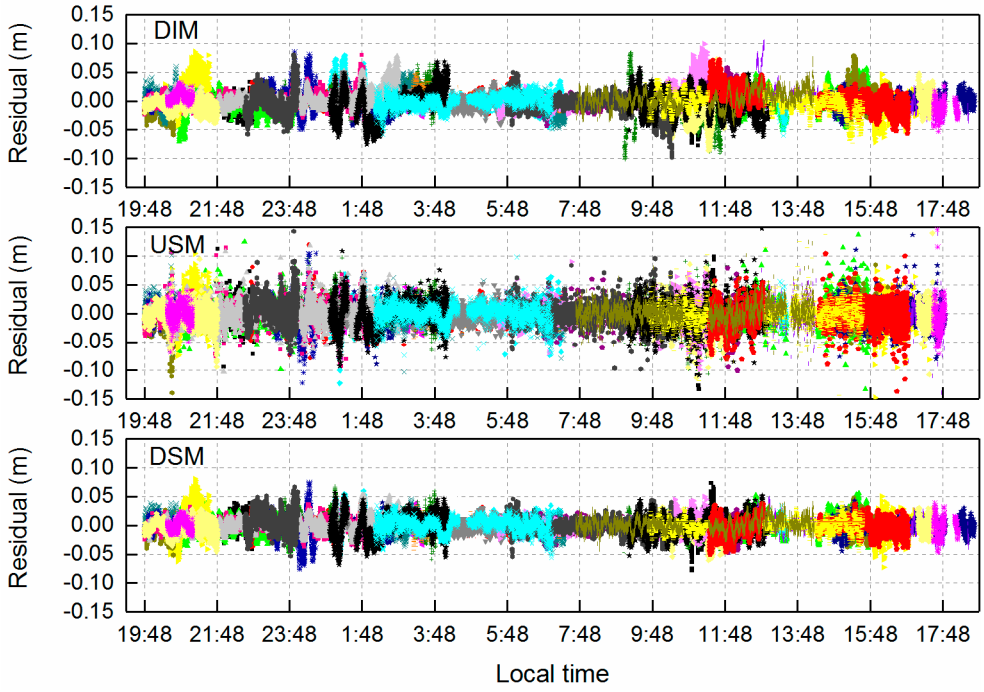

Figure 2. Time series of SD ionospheric residuals of DIM/USM/DSM in scenario A. Different colors represent SD ionospheric residuals of different satellite pairs.

Table 2. Accuracy of SD ionospheric delay interpolation for different interpolation methods (cm).

Model	Scenario							
	A		B		C		D	
	STD	RMS	STD	RMS	STD	RMS	STD	RMS
DIM	1.8	1.8	4.3	4.3	2.9	2.9	1.8	1.8
USM	1.8	1.8	4.9	4.9	2.9	2.9	-	-
DSM	1.4	1.4	3.2	3.2	2.2	2.2	1.4	1.4

Compared with DIM, DSM fully considered the variation in the ionospheric delay of each satellite pair in different directions, so the interpolation accuracy was better than that of DIM. The USM equation was correlated, which may have led to a decline in the interpolation of atmospheric delay.

According to the existing models, at least three reference stations are typically needed to interpolate the ionospheric delay. When three reference stations were used in scenario D, the interpolation accuracy of DIM and DSM did not change compared with when four reference stations were used, indicating that the server could still try to provide ionospheric corrections with just three reference stations. In contrast, USM could not provide service because the number of reference stations was insufficient.

As with the RMS values, the STD values of DSM are also relatively small, which reflects the good stability of the interpolation results, as shown in Table 2. In addition, the RMS and STD values for DSM were equal for the different scenarios, indicating that there was no systematic error in the interpolation ionospheric delay residual of the model.

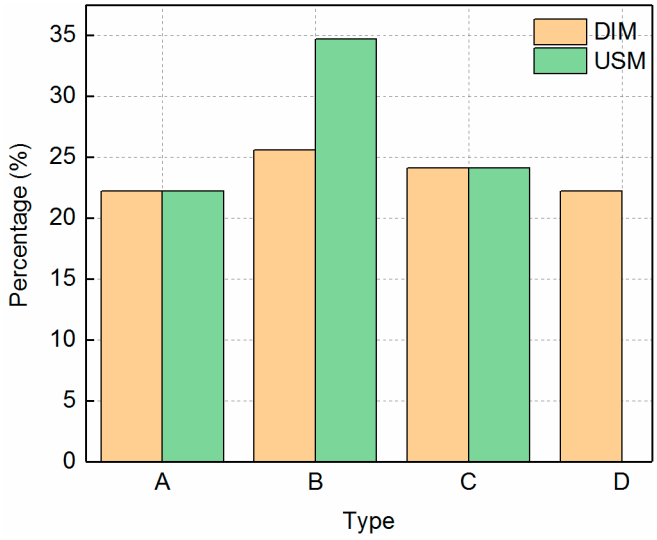

Figure 3. Percentage of interpolation accuracy improvement of DSM compared with USM and DIM in different scenarios.

4.2. Performance Analysis of PPP-RTK

According to the above analysis, the interpolation accuracy of DSM was the best among the interpolation methods that were tested, followed by DIM. Therefore, DIM was selected for comparison with DSM in PPP-RTK positioning performance for typical medium- and large-scale reference networks. During the experimental observation period from UTC 1:00 to 23:30, the PPP solution was reset every 5 min for the GPS and Galileo dual-system observation data. Each solution lasted for 5 min, resulting in a total of 270 groups of data. The atmospheric delays for the service end were modeled for each epoch, and the sampling interval was 5 s. The widely used ratio test was adopted as the quality control standard with IAR. The time to first fix (TTFF) was defined as the time that was required for the ratio value to be greater than 2, for the horizontal direction to be less than 5 cm, and for the vertical direction to be less than 10 cm in 20 consecutive epochs. When the TTFF was less than 5 min, the ambiguity was considered to be fixed successfully. The percentage of convergence time is defined as the ratio of the number of convergence periods to the number of successfully fixed periods. The initial variance of atmospheric delay is the key to the rapid convergence of PPP-RTK. The mean squared errors of the undifferenced ionospheric delays were 2 cm and 4 cm in scenarios A and B, respectively, with the empirical linear function [24], and the mean squared errors of the tropospheric delays were 1.5 cm and 2.5 cm [25] in scenario A and B, respectively. The tropospheric delay model used the LSM with first-order horizontal and vertical coordinates.

4.2.1. Medium-Scale Networks

The accuracy of SD ionospheric delay interpolation in scenario A was analyzed as described in Section 4.1. The average RMS of the residuals was 0.014 m for GPS and 0.012 m for Galileo using DSM. The interpolation accuracy of the two systems was similar. The RMS of the residuals for both GPS and Galileo was 0.018 m using DIM. The mean squared error of the SD ionospheric delays of 2.8 cm by experience is slightly larger than the situation. It is because the quality of the corrections of the surrounding reference stations should be much better than that of the single base station. Considering that too tight constraints will reduce the accuracy of the results, we think the empirical value that was used is appropriate, but it may not be optimal for all periods. Table 3 summarizes the convergence of the two models in the horizontal and three-dimensional directions. The horizontal success rate of DSM was approximately 95%, and the average convergence time was 14.5 s. Compared with DIM, the ambiguity fixation with DSM increased, but there was no significant difference in either TTFF or the percentage of convergence time. In the three-dimensional direction, 90% of

the periods converge within 1 min, 95% within 2 min, and all periods within 3 min using DSM. The convergence speeds of the two models in the horizontal direction were similar to those in the three-dimensional direction. To show convergence throughout the day, taking the DSM as an example, Figure 4 shows a time series diagram of TTFF in all periods and the number of satellites participating in ambiguity fixing at TTFF. When not converging, TTFF was set to −1. It can be seen that most of the periods with poor convergence are concentrated in the period with large ionospheric residuals in Figure 2. Except for the period with more ionosphere activity, during periods of the low number of satellites, the time that was required to fix the ambiguity was also longer. If the observation conditions were poor or the atmospheric delay products that were provided by the server were few, the number of satellites will be less, and the geometry of the satellite network will be poor. This will lead to poor solutions and ambiguity fixation failure. Therefore, multi-GNSS and multi-frequency observation data can be used to improve the performance of PPP-RTK, especially in urban areas with poor observation environments.

Table 3. Statistics of PPP-RTK simulating dynamic convergence results in the medium-scale networks.

Model	Coordinate	Fixing Percentage (%)	TTFF (s)	Percentage (%)		
				1 min	2 min	3 min
DIM	horizontal	93.7	13.6	91.3	96.8	99.6
DSM		95.2	14.5	89.9	95.3	100
DIM	three-dimensional	93.0	14.1	90.8	96.8	99.6
DSM		94.4	14.2	90.2	95.6	100

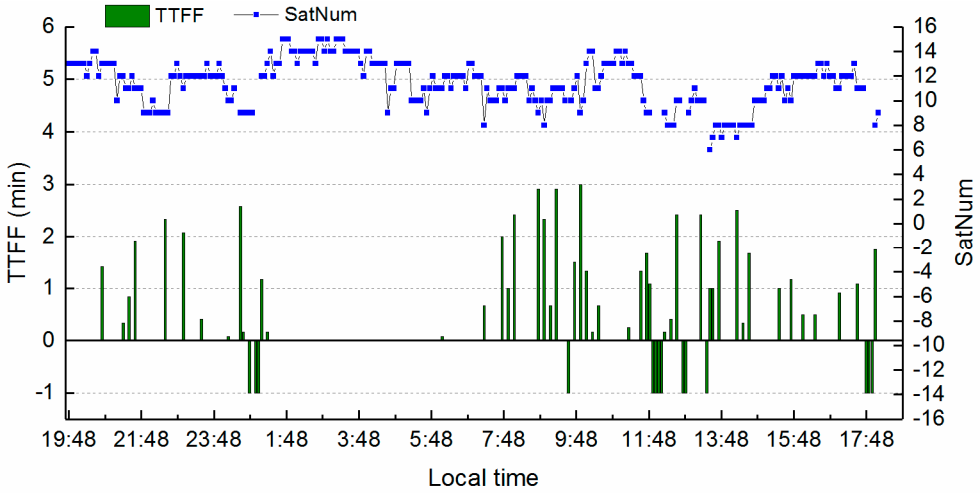

Figure 4. Time series of TTFF and satellite numbers with participating ambiguity-fixed satellites.

To explore the positioning accuracy after the ambiguity is successfully fixed, Figure 5 shows the positioning bias of the three directions (east, north, and up) at the TTFF. The horizontal bias of the DSM was concentrated within 2 cm, and the vertical bias was concentrated within 10 cm, while the DIM was less accurate than the DSM in the N direction. Figures 6 and 7 show the RMS value and its distribution of the positioning bias after the successful fixation in each period. The RMS was within 5 cm in the horizontal direction and within 10 cm in the vertical direction for all periods after convergence using the two models. However, the RMS values that were obtained using DSM of more than 90% and 98% of the horizontal bias were less than 2 cm and 3 cm, respectively. Approximately 66% and 93% of the vertical bias was less than 3 cm and 5 cm, respectively, and 98% was less than 10 cm, which was better than the results that were obtained using DIM. According to statistics, the average RMS values of the DSM in the three directions (E, N, U) were 0.80,

0.93, and 2.72 cm, which represent a reduction of 11.6%, 28.8%, and 10.6% compared with DIM, respectively.

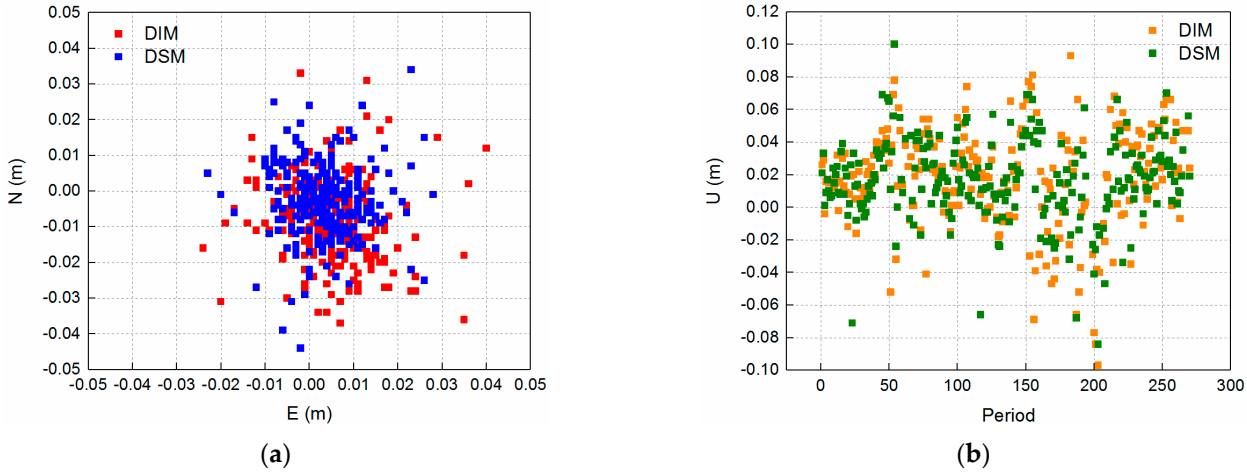

Figure 5. Positioning bias in (**a**) horizontal direction and (**b**) vertical direction at TTFF.

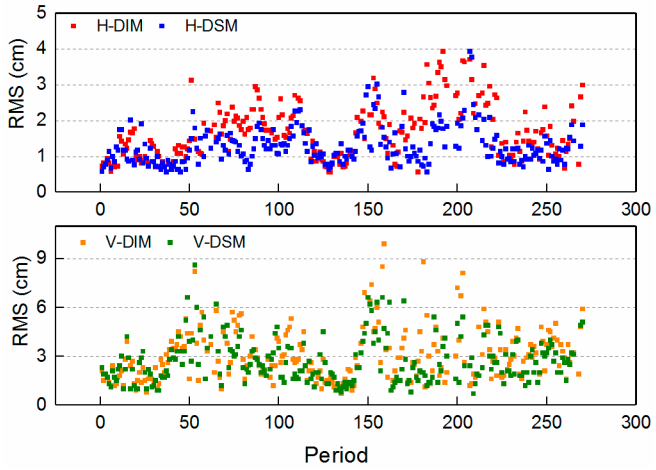

Figure 6. RMS values of horizontal (H) and vertical (V) directions after convergence.

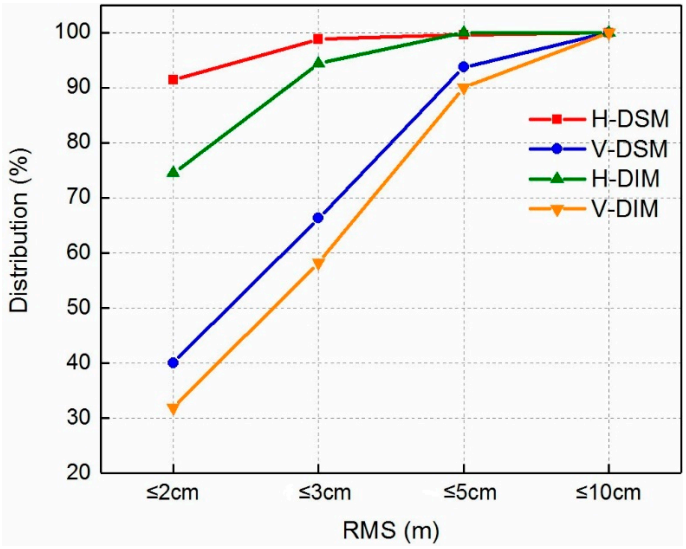

Figure 7. Distribution of RMS values in horizontal and vertical directions.

4.2.2. Large-Scale Networks

The SD ionospheric residuals of GPS and Galileo for the 98-km reference network are shown in Figure 8. The average RMS values of GPS and Galileo residuals that were interpolated by DSM were 0.032 m and 0.036 m, respectively. The average RMS values of GPS and Galileo residuals that were interpolated by DIM were 0.043 m and 0.045 m, respectively. The mean squared error of the SD ionospheric delays of 5.7 cm by experience is slightly higher than the interpolation accuracy. The SD ionospheric residual was poor during 9:00–14:00 local time throughout the observation period. The ionospheric correlation was weakened by the large distance between the user and reference station. Therefore, the interpolation accuracy was significantly reduced, especially during the active period of the ionosphere. The convergence of the two models in the horizontal and three-dimensional directions are summarized in Table 4. The TTFF of PPP-RTK for users in the 98-km reference network was 33.1 s. Using DSM, 77% of the periods converged within 1 min, 89% converged within 2 min, and 97% converged within 3 min. The convergence speed of DSM in the horizontal direction is similar to that in the three-dimensional direction, and so is the DIM. The ambiguity fixing rate for DSM was much higher than that for DIM, especially in the three-dimensional direction. For DSM, the ambiguity fixing rate in the horizontal direction was approximately 84%, and that in the three-dimensional direction was 82%. These represent 15.2% and 17.5% improvements, respectively, over those for DIM. The TTFF of DSM is faster than that of DIM. Figure 9 shows the positioning bias in the E/N/U direction at TTFF and the RMS value of the positioning bias after convergence in all periods. It can be seen from Figure 8 that the interpolation accuracy of DSM is better than that of DIM during the period of greater ionospheric activity. The maximum differences in the ambiguity between the two models occurred in the groups in the 165–195, that is, during the period with larger ionospheric residuals. During the same period, the positioning bias at TTFF was concentrated within 2 cm in the horizontal direction and 10 cm in the vertical direction. According to statistics, the average RMS values of DSM in the three directions (E/N/U) were 1.0, 1.1, and 4.0 cm, respectively compared with DIM, which represents a reduction of 8.2%, 29.2%, and 11.2%, respectively.

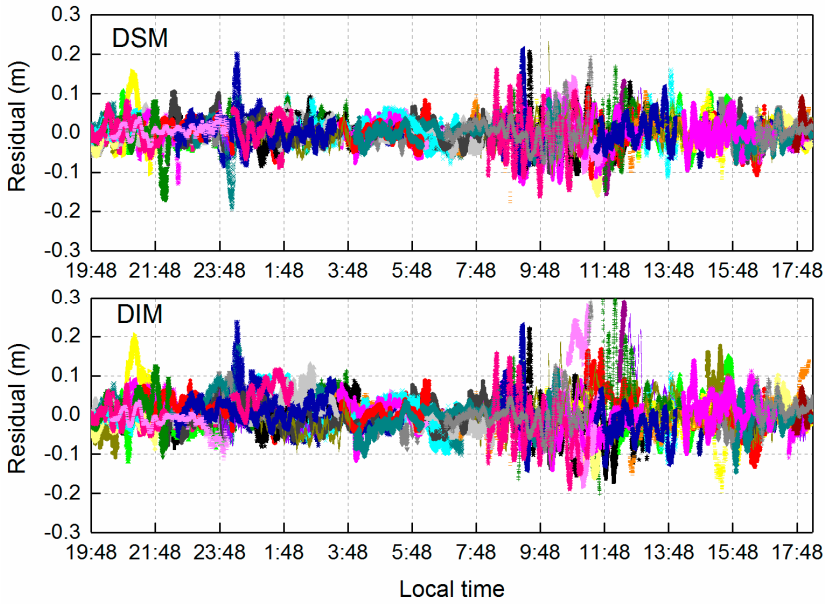

Figure 8. Time series of SD ionospheric residuals of DIM and DSM in large-scale networks. Different colors represent SD ionospheric residuals of different satellite pairs.

Table 4. Statistics of PPP-RTK simulating dynamic convergence results for large-scale networks.

Model	Coordinate	Fixing Percentage (%)	TTFF (s)	Percentage (%)		
				1 min	2 min	3 min
DIM	horizontal	71.9	46.3	67.5	89.2	98.9
DSM		84.8	30.4	78.2	91.3	97.8
DIM	three-dimensional	67.8	48.9	65.4	88.5	98.9
DSM		82.2	33.1	77.0	89.2	97.3

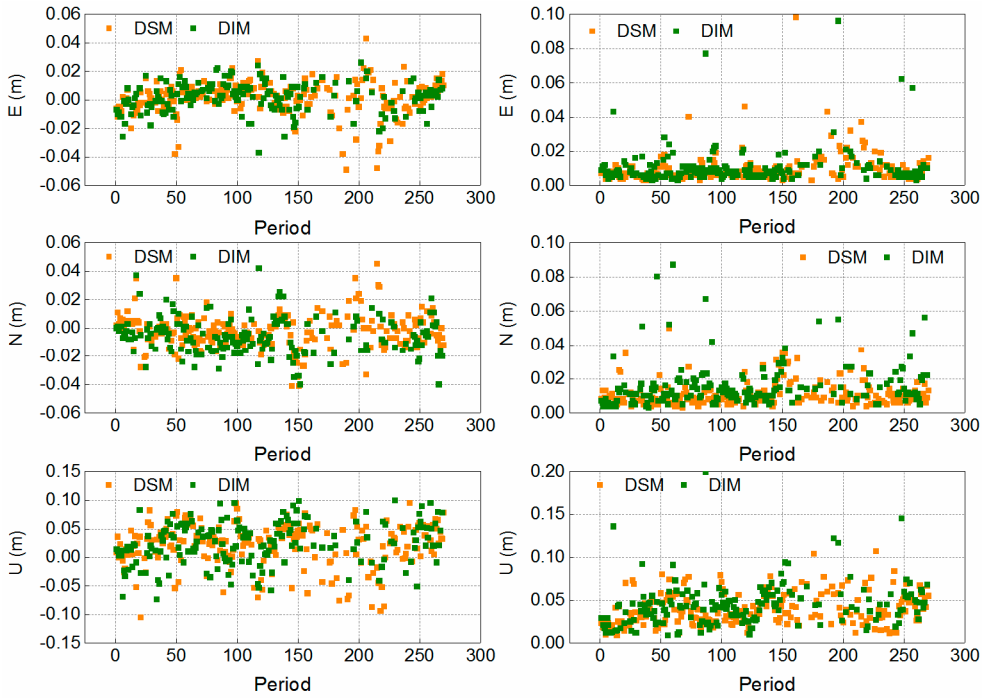

Figure 9. Positioning bias at TTFF (**left**) and RMS values after convergence (**right**) for large-scale networks.

5. Discussion

The DSM uses the mean position of each satellite pair's IPP and the intermediate position of the network to interpolate the ionospheric delay of users, which takes the variation in the ionospheric delay of each satellite pair in different directions into account fully and is easy to implement. The interpolation accuracy of DSM is better than that of DIM and USM, which are 1.4 cm, 3.2 cm, 2.2 cm, and 1.4 cm, respectively, in four scenarios. Compared with DIM whose interpolation accuracy is second only to the DSM, the interpolation accuracy represented improvements of 22.2% and 25.6% in the medium-scale and large-scale networks, respectively. What is more, for the scenario with three reference stations, the interpolation accuracies of DIM and DSM were no different from those for four reference stations, indicating that the server can still try to provide ionospheric correction service under the condition of fewer reference stations. In contrast, USM could not provide service because it lacked a sufficient number of reference stations. For users, the most concerning problem is the positioning performance after using interpolation correction. When the mean squared errors of the ionospheric delays by experience were determined and matched the interpolation accuracy basically on the whole, the positioning performance of DSM was better than that of DIM, especially in the large-scale networks. Hence, the DSM provides a reference for using the atmospheric delay coefficient based on the IPP to characterize the SD ionosphere delay, which can advance the application of PPP-RTK.

6. Conclusions

The interpolation model that was used for regional corrections is one of the key algorithms in a regional network ground-based enhanced positioning system. This paper proposes an SD ionospheric delay interpolation model for use with ionospheric corrections that are provided by the server in PPP-RTK technology through fixed ambiguity. CORS data from the United States were used together with a GPS as an example to analyze the interpolation accuracy of the proposed interpolation for four scenarios: a medium-scale reference network, a large-scale reference network, out-of-network users, and a network with a minimum of three reference stations. There were two typical scenarios of medium-scale and large-scale reference networks that were selected to analyze the PPP-RTK positioning performance of the model when constrained by atmospheric parameters. The PPP solution was reset every 5 min for the GPS and Galileo dual-system observation data. Each solution lasted for 5 min, and a total of 270 groups of data were analyzed. The conclusions that were drawn from the study results are as follows:

(1) The accuracy of the interpolation model decreases as the distance between the reference stations increases. The RMS values of the SD ionospheric delay residuals of DSM for the 41-km and 98-km reference networks were 1.4 cm and 3.2 cm, respectively. The interpolation accuracy of DSM was better than that of DIM and USM in both scenarios. When the user station outside the network was 33 km away from the nearest reference station, the RMS of ionospheric residual using DSM was 2.2 cm, which is better than that for DIM and USM under the same conditions. Unlike DIM, DSM takes the variation in the ionospheric delay of each satellite pair in different directions into account fully, so the interpolation accuracy is better than that of DIM. A correlation was obtained using USM in the test, which resulted in the inaccurate interpolation of atmospheric delay in some epochs. The RMS and STD values for DSM were equal in the different scenarios that were considered, which suggests that there is no systematic error in the ionospheric delay residuals using the new model.

(2) When there are three reference stations, the interpolation accuracies that were achieved with DIM and DSM were unchanged compared with those for four reference stations. This indicates that the server can still try to provide ionospheric corrections service under the condition of fewer reference stations, whereas USM cannot provide service due to the lack of enough reference stations.

(3) Under the condition that the same empirical model is used for the mean square error of atmospheric delay, the TTFF of PPP-RTK for users in the 41-km reference network was 14.5 s using DSM, with 90% of the periods converging within 1 min, 95% converging within 2 min, and all periods converging within 3 min. Compared with that of DIM, the ambiguity fixation of DSM was greater. After convergence, the mean RMS values in the E, N, and U directions were 0.80, 0.93, and 2.72 cm, respectively, which represented a reduction of 11.6%, 28.8%, and 10.6%, respectively, compared with DIM. The fixing rate of ambiguity of DSM was much higher than that of DIM for large-scale networks, especially in three dimensions. The fixing rate of ambiguity in the horizontal direction with DSM was approximately 84% and that in three dimensions was 82%, which are 15.2% and 17.5% higher, respectively, than those for DIM, and the TTFF of DSM is significantly faster than that of DIM. Using DSM, the TTFF for the 98-km reference network was 33.1 s, 77% of the periods converged within 1 min, 89% converged within 2 min, and 97% converged within 3 min. After convergence, the mean RMS values in the E, N, and U directions were 1.0, 1.1, and 4.0 cm, respectively, representing a reduction of 8.2%, 29.2%, and 11.2%, respectively, compared with DIM.

However, the interpolation accuracy of DSM is still relatively low when the ionosphere is relatively active, and it is necessary to further improve PPP-RTK positioning performance by optimizing the interpolation model, the stochastic model, or choosing the right number of stations, etc. At the same time, considering the development of multi-GNSS, the contribution of multiple GNSS, multiple frequencies, and precise atmospheric constraints to PPP deserves further exploration.

Author Contributions: J.H. and R.T. provided the initial idea for this work and write this manuscript; J.H. designed the algorithm. J.H., R.T., S.Z. and F.L. contributed to the analyses of results. F.L. and X.L. contributed to the collection and analysis of field test data. M.L. and R.T. drew the pictures. All authors have read and agreed to the published version of the manuscript.

Funding: This research was funded by the National Natural Science Foundation of China, grant number 41974032.

Acknowledgments: The authors gratefully acknowledge NOAA's National Geodetic Survey, IGS and GFZ for providing CORS network data and precision products.

Conflicts of Interest: The authors declare no conflict of interest.

References

1. Li, X.; Ge, M.; Zhang, H.; Wickert, J. A method for improving uncalibrated phase delay estimation and ambiguity-fixing in real-time precise point positioning. *J. Geod.* **2013**, *87*, 405–416. [CrossRef]
2. Wübbena, G.; Schmitz, M.; Bagge, A. PPP-RTK: Precise point positioning using state-space representation in RTK networks. In Proceedings of the ION GNSS, Long Beach, CA, USA, 13–16 September 2005.
3. Zhang, B.; Teunissen, P.; Odijk, D. A novel un-differenced PPP-RTK concept. *J. Navig.* **2011**, *64*, S180–S191. [CrossRef]
4. Wanninger, L. Improved ambiguity resolution by regional differential modelling of the ionosphere. In Proceedings of the 8th International Technical Meeting of the Satellite Division of The Institute of Navigation (ION GPS 1995), Palm Springs, CA, USA, 12–15 September 1995.
5. Gao, Y.; Li, Z.; McLellan, J.F. Carrier phase based regional area differential GPS for decimeter-level positioning and navigation. In Proceedings of the Institute of Navigation's ION GPS-97, Kansas City, MO, USA, 16–19 September 1997.
6. Han, S.; Rizos, C. GPS network design and error mitigation for real-time continuous array monitoring systems. In Proceedings of the Institute of Navigation's ION GPS-96, Kansas City, MO, USA, 17–20 September 1996.
7. Han, S.; Rizos, C. An instantaneous ambiguity resolution technique for medium-range GPS kinematic positioning. *Navigation* **2000**, *47*, 17–31. [CrossRef]
8. Fotopoulos, G. Parameterization of carrier phase corrections based on a regional network of reference stations. In Proceedings of the Institute of Navigation's ION GPS-2000, Salt Lake City, UT, USA, 19–22 September 2000.
9. Wübbena, G.; Bagge, A.; Seeber, G.; Boder, V.; Hankemeier, P. Reducing distance dependent errors for real-time precise DGPS applications by establishing reference station networks. In Proceedings of the Institute of Navigation's ION GPS-96, Kansas City, MO, USA, 17–20 September 1996.
10. Marel, H. Virtual GPS reference stations in The Netherlands. In Proceedings of the Institute of Navigation's ION GPS-98, Nashville, TN, USA, 15–18 September 1998.
11. Odijk, D.; Marel, H.; Song, I. Precise GPS positioning by applying ionospheric corrections from an active control network. *GPS Solut.* **2000**, *3*, 49–57. [CrossRef]
12. Krige, D.G. A Statistical Approach to Some Mine Valuations and Allied Problems at the Witwatersrand. Master's Thesis, University of Witwatersrand, Johannesburg, South Africa, 1951.
13. Liao, X. Carrier Phase Based Ionosphere Recovery Over a Regional Area GPS Network. Ph.D. Thesis, University of Calgary, Calgary, AB, Canada, 2001.
14. Dai, L.; Han, S.; Wang, J.; Rizos, C. Comparison of interpolation algorithms in network-based GPS techniques. *Navigation* **2004**, *50*, 277–293. [CrossRef]
15. Wang, S.; Li, B.; Gao, Y.; Gao, Y.; Guo, H. A comprehensive assessment of interpolation methods for regional augmented PPP using reference networks with different scales and terrains. *Measurement* **2020**, *150*, 107067. [CrossRef]
16. Li, X.; Zhang, X.; Ge, M. Regional reference network augmented precise point positioning for instantaneous ambiguity resolution. *J. Geod.* **2011**, *85*, 151–158. [CrossRef]
17. Zhu, Y.; Tan, S.; Ming, F.; Cui, X. IDW ionospheric TEC interpolation and accuracy analysis considering latitude and longitude anisotropy. *Geomat. Inf. Sci. Wuhan Univ.* **2019**, *44*, 1605–1612.
18. Cui, J.; Tang, W.; Jin, L.; Deng, C.; Zou, X.; Gu, S. An improved ionosphere interpolation algorithm for network RTK in low-latitude regions. *GPS Solut.* **2018**, *22*, 109. [CrossRef]
19. Wu, G.; Chen, J.; Wu, X.; Hu, J. Modeling and assessment of regional atmospheric correction based on undifferenced and uncombined PPP-RTK. *Acta Geod. Artograph. Sin.* **2020**, *49*, 1407–1418.
20. Leick, A.; Rapoport, L.; Tatarnikov, D. *CPS Satellite Surveying*, 4th ed.; Wiley: Hoboken, NJ, USA, 2015.
21. Tu, R.; Ge, M.; Zhang, H.; Huang, G. The realization and convergence analysis of combined PPP based on raw observation. *Adv. Space Res.* **2013**, *52*, 211–221. [CrossRef]
22. Zhang, B.; Zhao, C.; Odolinski, R.; Liu, T. Functional model modification of precise point positioning considering the time-varying code biases of a receiver. *Satell. Navig.* **2021**, *2*, 11. [CrossRef]
23. Wang, J.; Huang, G.; Yang, Y.; Zhang, Q.; Gao, Y.; Zhou, P. Mitigation of short-term temporal variations of receiver code bias to achieve increased success rate of ambiguity resolution in PPP. *Remote Sens.* **2020**, *12*, 796. [CrossRef]

24. Odijk, D. Weighting ionospheric correction to improve fast GPS positioning over medium distances. In Proceedings of the ION GNSS 2000, Alexandria, VA, USA, 19–22 September 2000; Institute of Navigation: Alexandria, VA, USA, 2000.
25. Li, B.; Verhagen, S.; Teunissen, P. Robustness of GNSS integer ambiguity resolution in the presence of atmospheric biases. *GPS Solut.* **2014**, *18*, 283–296. [CrossRef]